Determining weather radar antenna pointing using signals detected from the sun at low antenna elevations

Asko Huuskonen, Finnish Meteorological Institute

and

Iwan Holleman, Royal Netherlands Meteorological Institute, KNMI

corresponding author:

Asko Huuskonen,

Finnish Meteorological Institute,

P.O.Box 503, FI-00101 Helsinki, Finland

email: Asko.Huuskonen@fmi.fi

Abstract

A method to determine the elevation and azimuth biases of the radar antenna using solar signals observed by a scanning radar is presented. Data recorded at low elevation angles, where the atmospheric refraction has a significant effect on the propagation of the radio wave, are used and a method to take the effect of the refraction into account in the analysis is presented. A set of equations is given by which the refraction of the radio waves as a function of the relative humidity can easily be calculated. Also, a simplified model for the calculation of the atmospheric attenuation is presented. The consistency of the adopted models for the atmospheric refraction and atmospheric attenuation is confirmed by data collected at a single elevation pointing, but over a long observing time. Finally, the method is applied to data sets based on operational measurements at FMI and KNMI, and elevation and azimuth biases of the radars are shown.

1. Introduction

The use of the radio frequency radiation of the sun for checking of the antenna alignment and of the sensitivity of the receiver chain is a well established method in weather radar maintenance, and radar manufacturers offer sun calibration tools as part of their software packages. In the literature, the calibration of the antenna pointing has been discussed, e.g., by Whiton *et al.* (1976) and Mano and Altshuler (1981) and more recently by Arnott *et al.* (2003), Darlington *et al.* (2003) and Huuskonen and Hohti (2004).

Whiton *et al.* (1976) presented a method where the sun is located by a manual search method until a maximum is found, and the pointing bias determined thus. The method was seen particularly useful for mobile radars, for which other methods were not available. The paper also contains a summary of some prior work. Also Arnott *et al.* (2003) discussed the determination of the pointing angles of a mobile radar. They used the sun signatures recorded in the observed data to determine the orientation of the radar truck in azimuth. Mano and Altshuler (1981) describe a method to determine the true elevation of target using observations on a calibration target, e.g., sun, radio source, or satellite, which is at the same apparent angle as the target. Both targets are assumed to be above the troposphere and hence the diffraction is equal for both.

The use of the radio frequency radiation of the sun for off-line calibration of the alignment of the antenna and the sensitivity of the receiver was mentioned a number of times at the AMS radar calibration workshop in 2001. The use of the

sun for the calibration of the alignment of the radar antenna was mentioned by Keeler (2001). Crum (2001) presented encouraging results of the receiver calibration of the entire NEXRAD radar network using the sun. Validation of the solar calibration method revealed that the obtained biases are consistent with field reports.

Darlington *et al.* (2003) showed that the antenna alignment can be monitored on-line without disturbing the operational scan using unprocessed polar data. They used the method for the checking of the azimuth pointing only, because the highest elevation of their scan was 4^{o}, and they wanted to avoid the region where the textbook formulae for the refraction might not be valid. Huuskonen and Hohti (2004) used data from elevations below 3^{o}, and presented a method where data from several elevations are used together to determine the elevation bias, assuming that the refraction of the radio waves is described well by the formula for the optical refraction. They pointed out that a single sun rise or sun set is sufficient for the determination of the elevation bias. Holleman and Beekhuis (2004) developed a method for checking the antenna pointing, i.e., both in azimuth and elevation, and for on-line monitoring of the sensitivity of the radar receiver based on the sun.

In the present paper we combine the methods of Huuskonen and Hohti (2004) and Holleman and Beekhuis (2004) in order to determine both the antenna azimuth and elevation from operational scan data. Furthermore, we show the impact of the refraction and the atmospheric attenuation and present (improved) methods to correct for these effects. Finally, results from the Finnish and Dutch weather radar networks are presented.

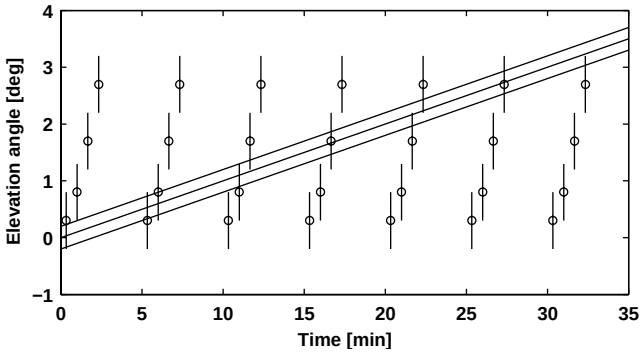

Figure 1: Hits of the radar antenna on the sun. A four elevation scan at 0.3°, 0.8°, 1.7°, and 2.7° elevations is performed at every 5 min. The antenna beam-width is plotted at each antenna position. The elevation of the sun center and of the sun edges is shown by solid lines, neglecting refraction.

2. Data and theory

a. Sun signatures

Weather radars scanning at low elevation angles regularly detect signals from the sun. These signals are most usually seen around sun rise and sun set and they can be recognized in the images as spokes in the direction of the sun. In the radar raw polar volume data the artifacts are observed whenever the antenna points close to the direction of the sun. The daily number of detected signatures depends on the season and the latitude of the radar, i.e., on the ascension/descent rate of the sun, on the solar activity, on the scanning strategy, and on the sensitivity of the receiver. This is illustrated in Fig. 1, which shows an example scan during the sun rise. Four elevations are scanned at every five min, and the sun rises from the horizon to 3° in about 30 min. During every scan, 1-2 sun hits are seen, in which

the antenna passes so close to the sun that the signature should be visible. In total we get approximately 10 hits during a sun rise.

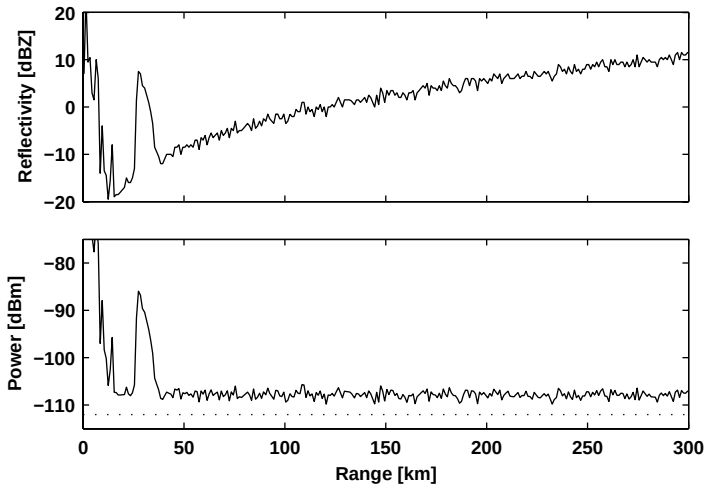

Figure 2: A-scope plot of the polar reflectivity data with a sun signal uncorrected (upper panel) and of the received power calculated applying the radar equation (lower panel). The noise level of the radar is indicated by the dashed line.

Figure 2 shows an example of the sun signature along the radar beam. The upper panel shows the calculated radar reflectivity as a function of range. The characteristic range dependence of the solar signal is clearly visible as the increase of the reflectivity with range. The received echo power is corrected for the range and for the atmospheric attenuation by the radar signal processor. The following equation is used by the processor to calculate the reflectivity in dBZ from the received power in dBm (SIGMET 1998):

$$dBZ = dBm + 20 \log R + 2aR + C, \tag{1}$$

where R is the range in km, a the one-way gaseous attenuation in dB/km and C

the radar constant in dB.

In the analysis of the solar signatures the received power is needed. Hence Eq. 1 is used in the backward direction to estimated the received power from the reflectivity. The application of the Eq. 1 is necessary because the solar data, in the signal processor, are processed as if they were reflections from the radar transmission. In the lower panel of Fig. 2 the received power calculated according to Eq. 1 is seen. The power is seen to be constant and above the noise level of the radar, and it evidently originates from a continuous source of radiation. The solar signal is strong in this case, which is a nearly exact hit to the sun. The strong signal at short ranges is ground clutter from the antenna side lobes, whereas the signal at about 30 km range is due to weather.

b. Atmospheric refraction

For the analysis of the solar signatures we have to know the position of the sun. The position of the sun, without the effect of refraction, is obtained from standard formulas (WMO 1996). The radiation of the sun is, however, refracted during its propagation through the atmosphere due to change of the refractivity with altitude. We are using radar data collected at very low elevations and, therefore, the refraction has to be taken into account. The magnitude of the refraction ϱ_t as a function of elevation can be described by the following equation (Sonntag 1989):

$$\varrho_t(el_t) = \frac{0.0045\ p_0}{T_0 \tan[el_t + 8.0/(el_t + 4.23)]} \tag{2}$$

where the refraction ϱ_t and the true elevation el_t are measured in degrees, and the temperature T_0 and pressure p_0 at ground level in Kelvin and hPa, respectively. The true elevation and apparent elevation el_a of the sun are related by:

$$el_a = el_t + \varrho_t(el_t) \quad (3)$$

$$el_t = el_a - \varrho_a(el_a) \quad (4)$$

where ϱ_a is the refraction as a function of the apparent elevation.

The equation of Sonntag (1989) is valid for visible light. The refraction of radio-frequency waves is expected to be stronger, because the refractivity depends also on the relative humidity U at these frequencies. The refractivity N for radio-frequency waves is given by (Doviak and Zrnić 1993):

$$\begin{aligned} N &= N = \frac{77.6}{T}(p + 4810\frac{p_w}{T}) \\ &= 77.6\,\frac{p}{T} + 3.7 \cdot 10^5 \frac{e_s(T)\,U}{T^2} \end{aligned} \quad (5)$$

where the total pressure p, the water vapor partial pressure p_w, and the water vapor saturation pressure e_s are given in hPa, $U = p_w/e_s$, and the temperature T is given in Kelvin. Assuming that Eq. 5 with $U = 0$ represents the refractivity at visible wavelengths, the refraction according to Sonntag (1989) can be rewritten as:

$$\varrho_t(el_t, N_0) = \frac{5.8 \cdot 10^{-5} N_0}{\tan[el_t + 8.0/(el_t + 4.23)]} \quad (6)$$

from which it is evident that the refraction as a function of the true elevation depends linearly on the refractivity at ground level N_0.

The refraction of visible light as a function of the apparent elevation is given

by (Sonntag 1989):

$$\varrho_a(el_a, N_0) = \frac{5.8 \cdot 10^{-5} N_0}{\tan[el_t + 6.3/(el_t + 4.0)]} \quad (7)$$

$$= \varrho_t(el_a - \varrho_a(el_a, N_0), N_0) \quad (8)$$

where Eq. 5 with $U = 0$ has again been used to introduce the refractivity N_0 at ground level. From the equations above, it is evident that the refraction as a function of the apparent elevation depends non-linearly on the refractivity.

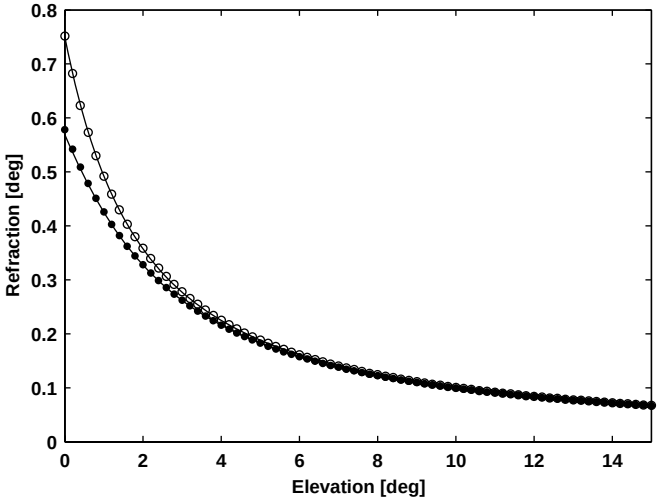

Figure 3: Refraction as the function of the true angle (open circles) and apparent angle (filled circles), calculated by the Starlink-SLA library, and the Sonntag-like curves fitted to the refraction points.

Refraction of C-band waves as a function of true and apparent elevation has been calculated using the "REFRO" routine of the Starlink-SLA library (CCLRC 2005). Refraction curves have been calculated for the 1976 US standard atmosphere (NOAA, NASA, USAF 1976), i.e., for an ambient temperature of 288.15 K,

a temperature lapse rate of 6.5 K/km, and a surface pressure of 1013.25 hPa. The refraction curves have been calculated for different relative humidities U and the resulting curves have been fitted to a Sonntag-like equation:

$$\varrho_i(el_i) = \frac{\alpha_i}{\tan[el_i + \beta_i/(el_i + \gamma_i)]} \tag{9}$$

where $i = t, a$ is indicating a function of either true or apparent elevation. Examples of the refraction curves calculated with the Starlink-SLA library and the curves fitted with the above equation are shown in Fig. 3. The resulting parameters $\alpha_i, \beta_i, \gamma_i$ have been further fitted to a polynomial function of U in order to have an analytic expression of the parameters for future reference.

For the true elevation case, only parameter α_t has been fitted because the refraction as a function of el_t scales linearly with the refractivity (see Eq. 6). Because α_t is a linear function of U (see Eq. 5) the result can be expressed as

$$\begin{aligned} \alpha_t(U) &= 0.0155 + 0.0054\,U \\ \beta_t(U) &= 8.00 \\ \gamma_t(U) &= 4.23 \end{aligned} \tag{10}$$

where the β_t, γ_t are also shown for completeness.

To minimize the number of fit parameters, $\alpha_a = \alpha_t$ was kept fixed during the fitting of the refraction as a function of the apparent elevation. In this case all parameters $\alpha_a, \beta_a, \gamma_a$ depend on the relative humidity and are given by

$$\begin{aligned} \alpha_a(U) &= 0.0155 + 0.0054\,U \\ \beta_a(U) &= 5.71 + 1.85\,U \end{aligned} \tag{11}$$

$$\gamma_a(U) \;\; = \;\; 3.42 + 2.11\,U + 0.19\,U^2$$

From the obtained values for α_i it follows that, depending on the relative humidity, the refraction of radio-frequency waves can be maximum 30% stronger than that of visible light.

c. Atmospheric attenuation

The atmospheric attenuation depends on the length of the path through the atmosphere and hence on the elevation of the antenna. A rigorous calculation takes into account the decay of the density with altitude, but a model where the density of the atmosphere is assumed constant up to an "equivalent height" z_0 and zero above is sufficient for our needs. Using the commonly applied $4/3$ earth's radius model (Doviak and Zrnić 1993), the range r from the radar can be written as a function of the apparent elevation el_a and the height z and the gaseous attenuation is then be approximated by:

$$A_{gas}(el_a) \simeq a{\cdot}r(z_0, el_a) = a{\cdot}\left(R_{43}\sqrt{\sin^2 el_a + \frac{2z_0}{R_{43}} + \frac{z_0^2}{R_{43}^2}} - R_{43}\sin el_a \right) \quad (12)$$

where R_{43} is the $4/3$ radius of the earth and a is the one-way gaseous attenuation at ground level in dB/km. The error due to this equivalent height approximation compared to using an exponential decaying density according to the 1976 US Standard Atmosphere is less than 8% for $el_a = 0$. The equivalent height z_0 of the atmosphere is chosen such that the integrated density is conserved:

$$z_0 \equiv \frac{1}{n_0}\int_0^\infty n(z)\,dz = \frac{p_0}{n_0 g} = \frac{RT_0}{g} \quad (13)$$

where the hydrostatic equation (Holton 1992) has been used to evaluate the integral. Symbol T_0 represents the atmospheric temperature at ground level, R the gas constant, and g is the gravitation constant. Using the temperature from the 1976 US Standard Atmosphere ($T_0 = 288.15$ K), an equivalent height of 8.4 km is obtained.

3. Data analysis method

The data used in the present study are obtained from the operational scans of the FMI and KNMI weather radars. The KNMI weather radars perform a 4-elevation reflectivity volume scan every 5 min using elevations of 0.3^o, 1.1^o, 2.0^o, and 3.0^o, and a 14-elevation reflectivity volume scan every 15 min using elevations of 0.3^o, 0.8^o, 1.3^o, 1.8^o, 2.3^o, 2.8^o, 3.3^o, 4.0^o, 5.0^o, 6.0^o, 7.5^o, 9.0^o, 10.5^o, and 12.0^o. The FMI weather radars use a similar scanning strategy, but for 9 elevations angles of 0.3^o, 0.8^o, 1.7^o, 2.7^o, 4.5^o, 6.0^o, 8.0^o, 11.0^o, and 20.0^o, of which the 4 lowest are repeated every 5 min.

Solar signals give rise to very distinct signatures in the polar data (see Fig. 2). Especially their extension to long ranges can be utilized for an automated detection procedure of the solar signals. The presence of a consistent reflectivity signal at long ranges, e.g., beyond 200 km, is the main signature used for identification of the solar signals.

Figure 4 shows a scatter plot of the solar signals collected by the weather radar in De Bilt. About 750 data points (all) have been collected during one month, and about 100 of them were classified as strong, i.e., received solar power higher than

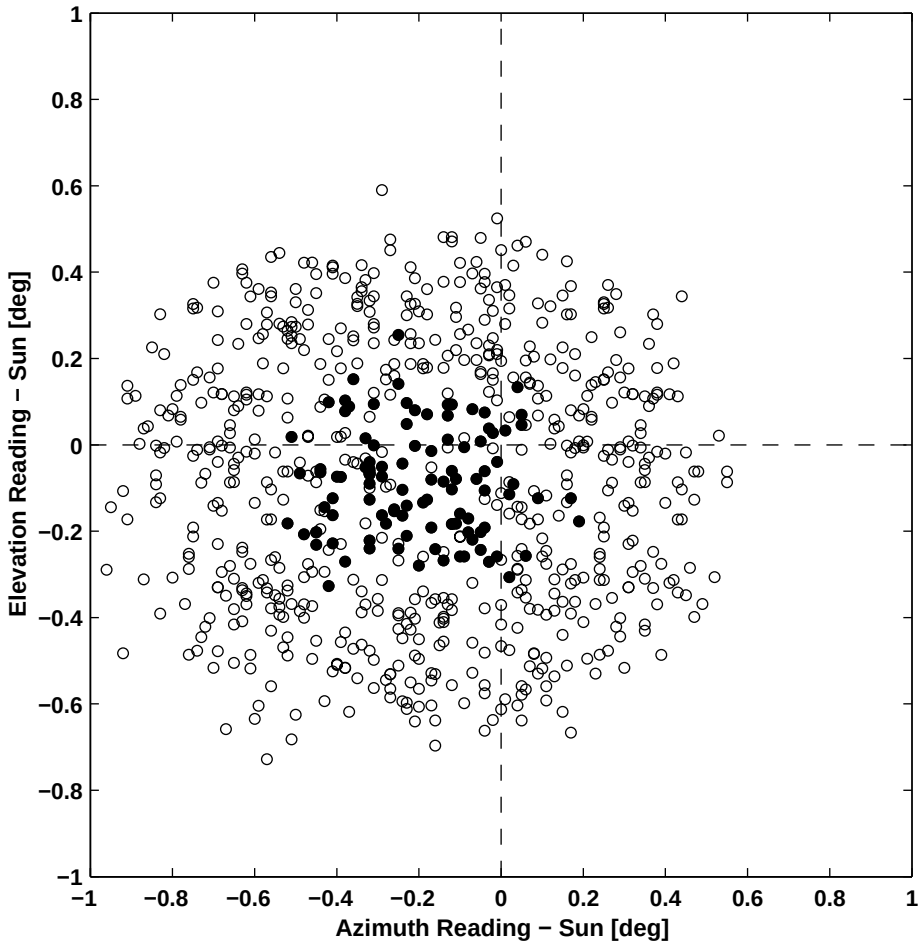

Figure 4: A scatter plot of the solar signals collected by the weather radar in De Bilt during March 2004. The vertical axis gives the difference between the observed antenna elevation (reading) and the calculated elevation of the sun, and the horizontal axis gives the same for the azimuth. The open circles show all solar hits, while the filled circles show the strong hits with a solar power higher than -108 dBm.

-108 dBm. It is evident from Fig. 4 that the solar signals are scattered over roughly 1° in both elevation and azimuthal direction. The width in azimuth is slightly larger because the antenna scan in azimuth produces additional smoothing not present in the elevation. Furthermore, it is evident that the strong solar signals are scattered over a much smaller area, i.e., about 0.5° in both directions, and that they are co-axial with all signals. These solar signals are evidently stronger because the sun and the radar antenna are better aligned in these cases. A small bias of the radar antenna in both elevation and azimuthal direction is exposed by the scatter plot analysis. This can be seen clearly from the large number of points in the lower-left quadrant of the scatter plot.

The solar signals with given elevation, azimuth, and received power collected over a predefined period can be analyzed using a numerical method and information on the biases of the antenna reading and the maximum solar power can be extracted. For this it is assumed that the errors in the antenna reading of azimuth and elevation are mainly due to bias errors. The azimuthal deviation x and elevation deviation y are defined as:

$$x = az_{read} - az_{sun} \tag{14}$$

$$y = el_{read} - el_{sun} \tag{15}$$

where (az_{read}, el_{read}) refer to the observed antenna angles and (az_{sun}, el_{sun}) to the calculated position of the sun. Before further analysis can be done, a shape for the solar power received by the antenna as a function of x and y needs to be assumed.

Assuming that the combination of the sun, antenna beam shape and the az-

imuthal beam averaging can be represented by a Gaussian form, the received solar power $p(x, y)$ in dBm can be written as:

$$p(x, y) = a_1 \cdot x^2 + a_2 \cdot y^2 + b_1 \cdot x + b_2 \cdot y + c \tag{16}$$

where it is important to note that this equation is linear in the parameters $a_{1,2}$, $b_{1,2}$, and c. The azimuth width Δ_{az}, the elevation width Δ_{el}, the azimuth bias x_0, the elevation bias y_0, and the maximum solar power p_0 can be calculated from the linear parameters:

$$\Delta_{az} = \sqrt{-\frac{40 \ {}^{10}\log 2}{a_1}} \tag{17}$$

$$\Delta_{el} = \sqrt{-\frac{40 \ {}^{10}\log 2}{a_2}} \tag{18}$$

$$x_0 = -\frac{b_1}{2a_1} \tag{19}$$

$$y_0 = -\frac{b_2}{2a_2} \tag{20}$$

$$p_0 = c - \frac{b_1^2}{4a_1} - \frac{b_2^2}{4a_2} \tag{21}$$

and naturally the widths can only be calculated when the corresponding parameter $a_{1,2}$ is negative.

Equation 16 is linear in the parameters a to c, and thus the solar signal data can easily be fitted to Eq. 16 by the least squares method. The resulting values for the parameters b_1, b_2, and c are then used to extract the biases and the maximum received solar power. The widths are often known, or can be calculated from the known properties of the antenna, sun and the scanning strategy. Hence they can be fixed in the fit in order to increase the stability of the fit and to reduce the number of points required.

In the operational use of the method, the solar signals collected over a certain period, typically a day, are analyzed using Eq. 16. The widths are kept fixed during the daily fit. The daily analysis is based on using data measured at several elevation pointings together. As the refraction of the radio frequency wave and the atmospheric attenuation both depend on the elevation pointing, these effects have to be taken into account, as given by Eqs. 9 and 12.

It is also possible to use data recorded at a single elevation angle but during several days to collect sufficient number of points for the fitting to succeed. Because the sun radiation power is not constant, one has to use the observed sun power to scale the data, or to select a period during which the sun radiation power does not change significantly. In that case we may neglect the refraction and attenuation in the fitting itself, because these effects are equally large for all the data points. We can then analyze the results over a set of elevation angles to study the validity the formulae for the atmospheric attenuation and for the refraction.

In the following we will first show single elevation analysis results and discuss the validity of our refraction and attenuation model and then show example results of the daily analysis.

4. Single elevation analysis

a. Atmospheric refraction

Figure 5 shows results from a fit of the Gaussian model to single elevation data (upper panel) and shows how the refraction model in Eq. 9 fits to our data (lower panel). The upper panel shows the elevation bias as a function of the antenna

elevation reading. The refraction is not included in the calculation of the sun position, and hence the difference is a combination of the effects of the refraction and the antenna pointing bias. The negative difference for large antenna elevations indicates an antenna offset, whereas the increasing difference with decreasing elevation is caused by the refraction.

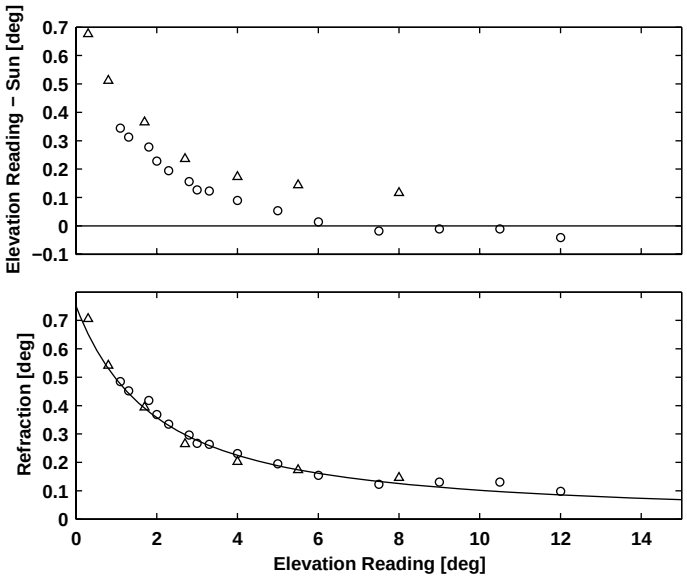

Figure 5: Upper panel: Difference of the elevation reading and the elevation of the sun neglecting refraction from the FMI data (triangles) and the KNMI data (circles). Lower panel: Refraction curve and observed data corrected for elevation bias.

The lower panel shows the data with the best fit elevation bias values.We fit the data to the equation

$$y = y_0 + \varrho_a(el_{read} + y_0) \tag{22}$$

where y is the difference of the elevation reading and the sun elevation, i.e. result

from the Gaussian fit, el_{read} is the antenna reading and y_0 is the antenna elevation bias. The equation is non-linear in the antenna bias and must be solved by least-squares fitting. It should be noted that we use here the refraction formula valid for the apparent angle el_a, which in turns depends on the antenna reading and elevation bias.

The best fit bias values are $-0.14^{\rm o}$ and $-0.03^{\rm o}$ for the KNMI data and the FMI data, respectively. As seen from the figure, the refraction curve calculated from Eq. 9 with parameters corresponding to a relative humidity of 0.6 fits very well to the observed data after bias correction.

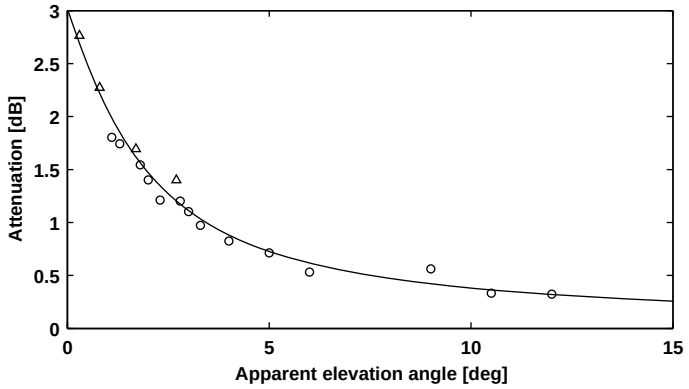

Figure 6: Atmospheric attenuation from theory (solid line), from FMI data (triangles) and from KNMI data (circles).

b. Atmospheric attenuation

Figure 6 shows the atmospheric attenuation determined from the FMI and KNMI data, together with the theoretical curve, calculated from Eq. 12. Because all our

data suffers from attenuation, even at the highest elevations, we have adjusted the data as follows. The KNMI data, which extends to an elevation of 12^o, is positioned so as to minimize the deviations from the theoretical curve at large elevations. The attenuation at the elevation of 12^o is less than 0.5 dB, so that any residual error remaining must be low. The FMI data, available only for the lowest elevations, is placed so as to fit to the curve best. Although our results do not give absolute attenuation values, the data confirms that the form of the curve is correct, i.e., the attenuation differences between two elevations follow the formula.

The amount of atmospheric attenuation depends on the elevation pointing, because the solar radiation travels longer in the atmosphere for lower elevations. We have adopted a simplified model in which the atmosphere is replaced by a layer with constant density. The approximation is correct to 8% or better. The data from a single elevation, but collected over a long time period, show that the observed solar flux as a function of elevation is consistent with the adopted model. This is important when data from several elevations is used together in the same fit.

5. Daily analysis results

It has been detailed in a previous section that the collected solar signals can be analyzed to obtain the azimuthal and elevation biases using a linear fit. In Fig. 7 the results of a daily analysis of the solar signals collected by the radar in De Bilt (52.10^o N, 5.18^o E) between 1 April and 31 May 2004 are shown. The upper frame shows the number of solar signals collected per day. During this period typically between 20 and 30 hits are detected each day.

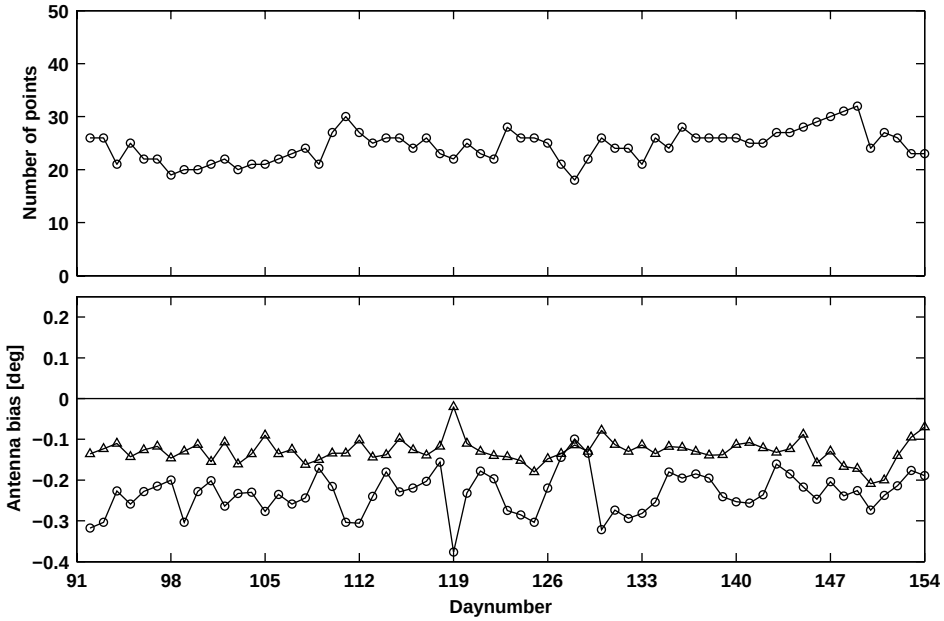

Figure 7: Results of the daily analysis of the solar detection from the radar in De Bilt in April and May 2004. The number of sun hits is given in the upper panel, and the extracted biases in azimuth (circles) and elevation (triangles) readings in the lower panel.

The lower frame of Fig. 7 shows the extracted biases of the azimuth and elevation readings of the radar antenna. It is evident from the figure that the extracted elevation bias is slightly negative and fluctuates between -0.1° and -0.15°. In order to have a correct height assignment of the radar observations, an elevation bias of maximum 0.1° is acceptable for operational weather radars. So the bias of the antenna elevation reading of De Bilt is apparently almost within acceptable limits. In addition, the ”noise” on the extracted elevation bias suggests that the random error on the elevation bias obtained from the solar signal data is less than 0.05°. The extracted azimuth bias is also negative but somewhat larger than the

elevation bias. It fluctuates between -0.1° and -0.3°. For a weather radar the azimuth bias is less critical than the elevation bias. When the geographical referencing of the radar data has to be accurate within 1 km at 200 km range, the bias in the azimuth reading of the antenna must be less than 0.3°. The random error on the azimuth bias obtained from the solar signal data appears to be less than 0.1°.

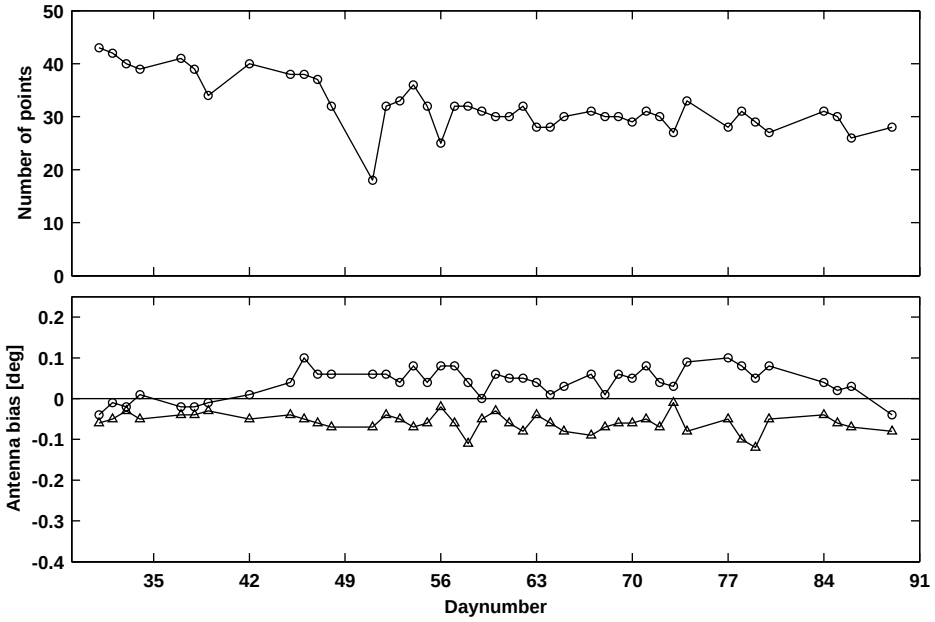

Figure 8: Results of the daily analysis of the solar detection from the radar in Kuopio in February and March 2005. The number of sun hits is given in the upper panel, and the extracted biases in azimuth (circles) and elevation (triangles) readings in the lower panel.

Figure 8 shows results of a daily analysis of the Kuopio radar (62.86° N, 27.39° E) of the FMI network. The panels are as in Fig. 7. In all main features the data from Kuopio confirm the findings from the KNMI De Bilt radar. The number of solar signals is slightly higher, which might indicate a better sensitivity of

the receiver, but is more probably explained by the more Northern location of the Kuopio radar. At higher latitudes the sun raises and sets at a lower rate, and thus the number of hits within a given elevation range is larger. Highest numbers are seen in Finland during the Summer and Winter solstices, and the Utajärvi radar (64.77^o N, 26.32^o E), which is 2^o south of the polar circle, observed as many as 120 sun hits per day around the winter solstice.

The lower panel shows that the elevation bias is about 0.05^o and the azimuth bias -0.05^o and that both have random error less the 0.05^o, in agreement with the result from De Bilt. A notable difference is that the result is not available for every day. The FMI results are based on low elevations, in which the rain may mask the sun signal altogether. The KNMI analysis utilizes also higher elevations, which contain data from altitudes above the rain, and the analysis results are obtained also during rainy days. The random error of the estimated bias is again less than 0.05^o, estimated from the random fluctuations of the bias curve.

6. Conclusions

The method of using detection of the sun to determine the elevation and azimuth biases of the radar antenna is well established, and the use of operational scan data of a scanning radar has been discussed by Arnott *et al.* (2003) and Darlington *et al.* (2003) for azimuth pointing and by Huuskonen and Hohti (2004) and Holleman and Beekhuis (2004) for the elevation pointing.

In this paper we have improved the method so that it can use operational radar scans made at very low elevation angles, where the atmospheric refraction has a

significant effect on the propagation of the radio frequency waves. For this end, a model is presented which gives the atmospheric refraction as a function of both the true sun elevation and the apparent sun elevation. The model is based on the refraction values for radio frequency waves, given by the Starlink library, which we have shown to follow the functional form as given by Sonntag (1989). The resulting equations facilitate the use of the refraction model in operational data analysis. The analysis of our radar data shows that the observed elevation biases are consistent with the refraction model.

We have also created a model which gives the atmospheric attenuation as a function of the radar elevation. The analysis of our radar data shows that the model explains the observed differences in the received power as a function of the elevation angle.

The operational scans both at FMI and KNMI measure a set of elevations every 5 min, and a larger set once every 15 min. During a sun rise or sun set some 10-15 sun hits are observed in the data, depending on season. The results show that the sun hits from one day are sufficient for the determination of the biases.

The effect of a bias in the antenna elevation is more severe at low antenna elevations. At long distances a small error in the elevation creates a large deviation in the altitude. This is increasingly important now that the quantitative use of radar data is increasing and profile correction methods are used to determine the effective radar reflectivity on the ground from a measurement made aloft. An error in the beam altitude produces an error in the deduced ground reflectivity and thus in the precipitation rate. With our method it is possible to determine the elevation

bias at the very low elevations in which the accurately known elevation is of most value. A determination of the antenna elevation bias at a high elevation, whilst easy and not dependent on the refraction model, is vulnerable to errors caused by antenna elevation reading non-linearities.

The antenna azimuth bias does not depend on the refraction model and thus the determination of the azimuth bias is free of the problems described above for the elevation. Our method gives both biases from a single fit.

7. Acknowledgments

The authors are indebted to Norman Donaldson from Environment Canada for pointing out the existence of the Starlink Project, as well as for valuable discussions on the subject. Hans Beekhuis (KNMI) is gratefully acknowledged for technical assistance and valuable discussions. The authors acknowledge the data analysis facilities provided by the Starlink Project which is run by CCLRC on behalf of PPARC.

References

Arnott, N. R., Y. P. Richardson, J. M. Wurman, and J. Lutz, 2003: A solar alignment technique for determining mobile radar pointing angles. *31st Conference on Radar Meteorology*, AMS, 491–493.

CCLRC, 2005: Starlink project. http://star-www.rl.ac.uk.

Crum, T., 2001: WSR-88D calibration: Changes and new approaches. *Workshop on Radar Calibration, Albuquerque NM*, AMS.

Darlington, T., M. Kitchen, J. Sugier, and J. de Rohan-Truba, 2003: Automated real-time monitoring of radar sensitivity and antenna pointing accuracy. *31st Conference on Radar Meteorology*, AMS, 538–541.

Doviak, R. J. and D. S. Zrnić, 1993: *Doppler Radar and Weather Observations*, Second edition. Academic Press, 562 pp.

Holleman, I. and H. Beekhuis, 2004: Weather radar monitoring using the sun. Technical Report TR-272, Royal Netherlands Meteorological Institute (KNMI), 40 pp.

Holton, J. R., 1992: *An introduction to dynamic meteorology*, Third edition. Academic Press, 511 pp.

Huuskonen, A. and H. Hohti, 2004: Using the solar flux data from operational scans for checking the elevation pointing of a radar. *3rd European Conference of Radar Meteorology and Hydrology (ERAD)*, EMS.

Keeler, R. J., 2001: Weather radar calibration. *Workshop on Radar Calibration, Albuquerque NM*, AMS.

Mano, K. and E. E. Altshuler, 1981: Tropospheric refractive angle and range error corrections utilizing exoatmospheric sources. *Radio Sci.*, **16**, 191–195.

NOAA, NASA, USAF, 1976: *U.S. Standard Atmosphere*. U.S. Government Printing Office, Washington D.C.

SIGMET, 1998: RVP6 Doppler signal processor user's manual. Sigmet, 2 Park Drive, Westford, MA 01886 USA.

Sonntag, D., 1989: *Formeln verschiedenen Genauigkeitsgrades zur Berechnung der Sonnenkoordinaten (Equations for calculation of the solar position with different accuracies)*. Abhandlungen des Meteorologischen Dienstes der DDR, no. 143, Akademie-Verlag, Berlin, 108 pp.

Whiton, R. C., P. L. Smith, and A. C. Harbuck, 1976: Calibration of weather radar systems using the sun as a radio source. *17th Conference on Radar Meteorology*, AMS, 60–65.

WMO, 1996: *Guide to Meteorological Instruments and Methods of Observation, No. 8*, Sixth edition. Secretariat WMO, Geneva, Switzerland, approx. 452 pp.